Proceedings of ISFOG 2025
5TH INTERNATIONAL SYMPOSIUM ON
FRONTIERS IN OFFSHORE GEOTECHNICS
Nantes, France | June 9-13 2025

ISBN 978-2-85782-758-0

Small and large scale model tests on suction caissons in sand under axial cyclic loading

I. Sanders*, M. Achmus
Leibniz University Hannover, Hannover, Germany

D. Heinrich, T. Quiroz
Fraunhofer-Institut für Windenergiesysteme, Hannover, Germany

W. Elsesser
GuD Geotechnik und Dynamik Consult GmbH, Berlin, Germany

sanders@igth.uni-hannover.de

ABSTRACT: At greater water depths, offshore wind turbines are often founded on jacket structures, which transfer the overturning moments from horizontal loads into the subsoil mainly as axial loads. Suction caissons (SC) can be used as alternative foundation elements to piles, and are installed into the subsoil by means of underpressure (suction), avoiding the generation of pile-driving noise. Due to the relatively low embedment, the drained tensile load-bearing capacity of SC is rather low. However, an underpressure is created during rapid tensile loading, which can significantly increase the tensile load-bearing capacity. A very relevant question for the design is to what extent cyclic tensile loading of suction caissons can be permitted without jeopardizing the serviceability of the foundation. This paper reports on 1g model tests of SC with diameters of D = [0.61, 1.60, 2.40] m in fine sand under cyclic axial loads. All SC were installed using suction to consider installation effects on the load-bearing behaviour. The results show that for alternating loads or loads with a mean load in the compression range, the permissible load amplitude depends on the load frequency and thus the drainage conditions. Cyclic loads with a tensile mean load above a certain threshold lead relatively quickly to progressive failure and should be avoided at all costs. Small sustained tensile mean loads lead to an accumulation of heave, but can – depending on load frequency and amplitude – be permitted for a limited number of cycles.

Keywords: Suction Caisson, Small Scale Model testing, Scaling, Pore water pressure

1 INTRODUCTION

Due to the weight of the superstructure, suction caisson foundations (also known as suction buckets) on offshore wind energy generators (OWEG) are subject to compressive loads under normal conditions. Under storm loads, the leeward caisson might be subjected to tensile loads. With OWEG being installed in deeper waters, it would be beneficial to allow small tensile loads to occur even outside of storm events. Since smaller load amplitudes are more likely to occur, higher numbers of load cycles are of particularly high interest for such loading conditions.

Loading that significantly exceeds the drained tensile capacity leads to ongoing severe upward displacements of suction caisson foundations (Byrne, 2000, Kelly et al., 2004, Gütz, 2020). Several studies found, that loading conditions which do not exceed the drained tensile capacity and have sufficient mean compressive loads do not lead to ongoing upward displacements, while cyclic loads with even zero or small tensile mean loads might do so (Bienen et al., 2018, Stapelfeldt et al., 2020, Vaitkunaite, 2016, Zhang et al. 2020). Zhang et al. (2020) observed initial settlements even for small tensile mean loads. These were attributed to recompaction of the soil that was loosened during suction installation.

Both Bienen et al. (2018) and Stapelfeldt et al. (2020) observed little to no pore water pressure accumulation under alternating loads not excessively exceeding the drained tensile capacity in centrifuge tests. Gütz (2020) conducted 1g small-scale model tests with pure tensile loads and observed purely increasing pore water pressure accumulations (suction) only for tests with a mean load exceeding the drained tensile capacity. Tests with mean loads below the drained tensile capacity showed initial decrease in accumulated pore water pressures.

In small-scale model tests at 1g, the stress-dependent stiffness of the soil is not increasing over the depth of the foundation as it would on the prototype scale. Additionally, dilation of the soil is stress-dependent and has greater impact in small models. When considering transient (e.g. consolidation-related) problems, drainage paths, pressure application areas and volumes change at

different rates (c.f. square-cube law). Major advantages of 1g model testing are the relation of the model size to grain size, which is usually greater than in centrifuge testing, cost-effectiveness and straight-forward implementation of tests.

Approaches for scaling of the load are mostly based on theoretical considerations and are shown in rearranged form for better comparability:

$$\frac{f_m}{f_p} = \frac{k_m}{k_p}\left(\frac{D_p}{D_m}\right)^{\beta} \qquad (1)$$

where k (m/s) is the hydraulic conductivity, f (Hz) is the loading frequency and D (m) is the diameter of the foundation. Indices m and p denote model and prototype properties, respectively.

Kelly et al. (2006) deduced $\beta = 3/2$ by employing the dimensionless time-parameter T_v. Lombardi et al. (2011) proposed $\beta = 1$ based on dimensional analysis and the general approach mentioned in Wood (2004) for similar hydraulic conductivities, i.e. $k_m / k_p = 1$, states $\beta = 1 - \alpha/2$ where $\alpha = 0.5$ for sand.

Gütz (2020) proposed a scaling approach by numerical modelling, where the achievement of similar displacement rates after several cycles is the expression for similar frequencies. This approach faces challenges when transferred to loads that are not purely tensile but might even under these conditions give valuable insights into the drainage conditions of the system.

Since no single approach for scaling exists and other effects of scaling are not considered in the existing approaches, this study investigates the comparability of 1g model tests that were conducted on a small and a large scale.

2 METHODS

2.1 Model test setup

For the small-scale model tests, a caisson with diameter and length of $D = L = 0.61$ m was tested in a cylindrical test container with diameter $D_S = 2.5$ m and height of the sand $H_S = 2.1$ m. Loads were applied via an electromechanical actuator. Figure 1 shows the setup used for the small scale model tests. The small-scale model testing procedure comprised a succession of soil loosening and compaction, suction installation of the model foundation, determination of drained tensile capacity $F_{dr,t}$ and application of cyclic load. Relative density of the soil prior to installation was in the range $D_r = 0.82 - 0.87$ and achieved installation depths were approximately $z_{end}/L = 0.92 - 0.94$. The contact between lid invert and soil surface was proven

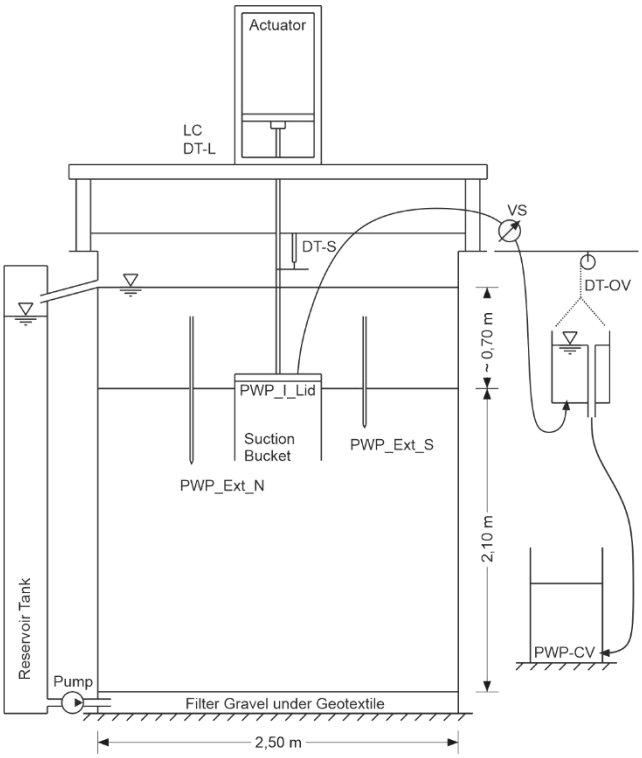

Figure 1. Testing facility for the small scale model tests. LC – Load cell, DT – Displacement transducer, PWP – Pore water pressure transducer, VS – volume flow sensor.

by stiffness increase during a last phase of the installation with constant displacement rate. A detailed overview of the installation procedure can be found in (Sanders and Achmus, 2023).

The large scale tests were carried out in a geotechnical testing pit with dimensions of the soil body $L_S = 14$ m, $W_S = 9$ m, and $H_S = 9.25$ m. Loads were applied via a hydraulic actuator. Figure 2 shows the setup used for the large scale model tests.

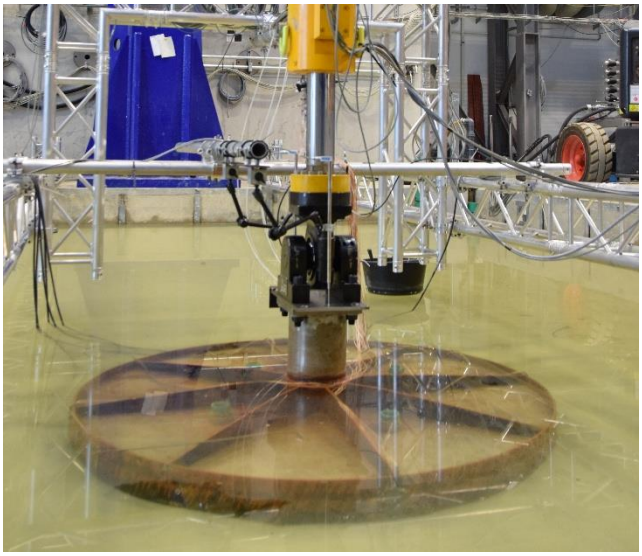

Figure 2. Testing facility for the large scale model tests, and specimen with D = 1.6 m.

Sand in the testing pit was installed and compacted in layers, the resulting relative density was $D_r = 0.64$. Caissons of two different diameters $D_1 = 1.6$ m and $D_2 = 2.4$ m and constant aspect ratio $L/D = 0.89$ were used. The installation procedure is described in detail in the companion paper (Heinrich et al., 2025).

Relative densities achieved in the soil preparation were confirmed by CPTs prior to caisson installation on both scales, and additionally by soil core samples on the large scale.

Table 1 shows the properties of the two fine silica sands that were used in the tests (small scale: *G12T*, large scale: *Rohsand 3152*). *Rohsand 3152* has higher content of fines and shows a slightly smaller hydraulic conductivity.

Table 1. Properties of the sands used in small (G12T) and large (Rohsand 3152) scale model tests.

Property		Unit	G12T	Rohsand 3152
Maximum void ratio	e_{max}	1	0.873	0.82
Minimum void ratio	e_{min}	1	0.553	0.41
Coefficient of uniformity	C_U	1	1.36	1.82
Coefficient of curvature	C_C	1	0.96	0.96
Hydraulic conductivity	k	m/s	2.5E-4	1.09E-04

2.2 Loading conditions

The small-scale model was used to carry out 35 tests, with cyclic force loading as well as constant displacement rate loading. The large scale suction caissons were installed one (D_2) and three (D_1) times, respectively.

The applied sinusoidal loads can be described by the frequency f, the mean load F'_m, and the load amplitude F'_a. For comparability, normalized loads will be used in the following, defined as $F' = F/|F_{dr,t}|$. Compressive loads, overpressures (compressive) and downward displacements are considered positive. Figure 3 shows the loading conditions for all model tests.

The initial loading rate was chosen as the maximum loading rate during the cyclic load.

$$(\delta F/\delta t)_{max} = f * F_{amp} * 2\pi \qquad (2)$$

Loading commenced in the direction of the mean load, and was compressive for tests with $F'_m = 0$.

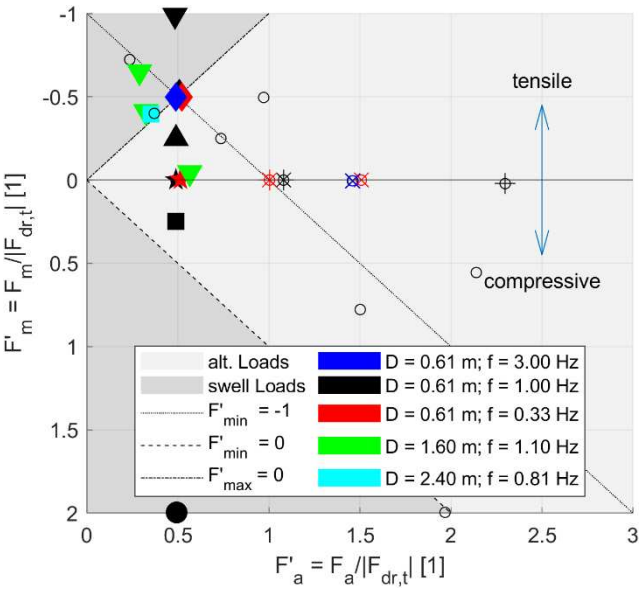

Figure 3. Load combinations employed in the model tests. Scaled to drained tensile capacity. Blue, black and red indicates frequencies of f = [3, 1, 0.33] Hz, respectively. Load combinations of large scale model tests displayed in green.

The loading frequency was f = 1 Hz in most small-scale tests (base case). Tests at certain significant loading conditions were repeated with additional frequencies of $f = [0.33, 3]$ Hz.

Only a single loading configuration was used for each small-scale model test. This allowed for loads to be chosen freely without consideration of influence on other load packages. During the large scale model tests, the highest tensile load was far below the drained tensile capacity in most tests to minimize impacts on the following load packages. Also, the drained tensile capacity was determined only prior to the first load package for large scale tests.

Frequencies for large scale model tests were calculated according to the approach from Wood (2000) to match a fictitious prototype foundation with $D_P = 9\ m$ and were $f_1 = 1.1$ Hz for D_1 and $f_2 = 0.81$ Hz for D_2.

Most scaling approaches account for varying hydraulic conductivities, which govern the drainage conditions. Since the exact determination of hydraulic conductivity is prone to uncertainties, the frequencies of the large scale model tests are considered to be of equal magnitude for this study.

3 RESULTS

3.1 Drained tensile capacity

Figure 4 shows the drained tensile capacity $F_{dr,t}$ normalized by the system properties as proposed by Hettler (1982) to yield the drained tensile resistance factor $k{\cdot}tan(\delta)$. For small-scale model tests, the mean bearing factor at $\Delta z/L = 0.0015$ was $k{\cdot}tan(\delta) = 0.273$ with a small standard deviation of $s = 0.01$.

Increased dilation at small scale governs the behaviour for 1g model testing. According to the results presented by Gütz (2020) the bearing factor for the small-scale model tests should be slightly lower than observed. Yet, some changes were made to the system (e.g. last stage of installation with constant displacement rate was added, cf. Gütz, 2020 and Sanders and Achmus, 2023). Counterintuitively, results for the large scale model tests show both increased stiffness at lower normalized displacements as well as higher bearing factors. This might be explained by differences in the used soil and preparation method.

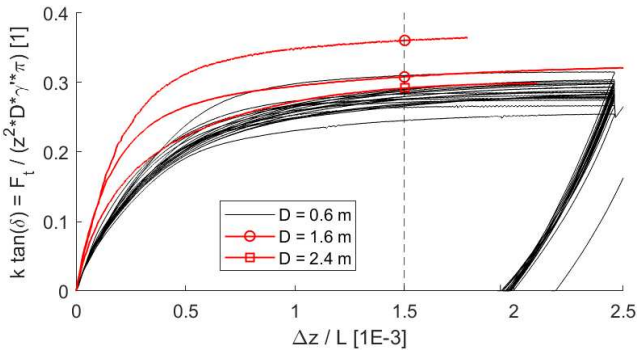

Figure 4. Activation of resistance factor k·tan(δ) for different scale model tests.

3.2 Displacements and pore water pressures

In the following, mean and amplitude displacements and pore water pressures are shown. Those values were obtained from the minimum and maximum values that occurred during each cycle. While a phase shift is present between load and pore water pressure, the relation of the respective impulses from load and equivalent pore water pressure force during each cycle showed a good correlation with the minimum and maximum values. Thus, the employment of these minimum and maximum values was deemed representative.

For small-scale tests, displacements were deduced for each cycle, pore water pressures for cycles with high resolution. For better overview, pore water pressure related values in plots will be connected by straight lines. On the large scale, data is shown for certain (single) representative loading cycles only.

Figure 5 shows the dependency of the vertical displacements on the loading conditions after $N = 1$ and $N = 10$ cycles. A clear influence of the mean load can be seen, while the loading amplitude did only have a subordinate influence on initial settlements. The same influence can be observed for the initial pore water pressures (not depicted). Since the initial loading rate was directly dependent on amplitude and frequency (c.f. Eq. 2), this implies that for the employed load combinations the mean load had higher impact on the bearing behaviour and the drainage conditions than the loading rate.

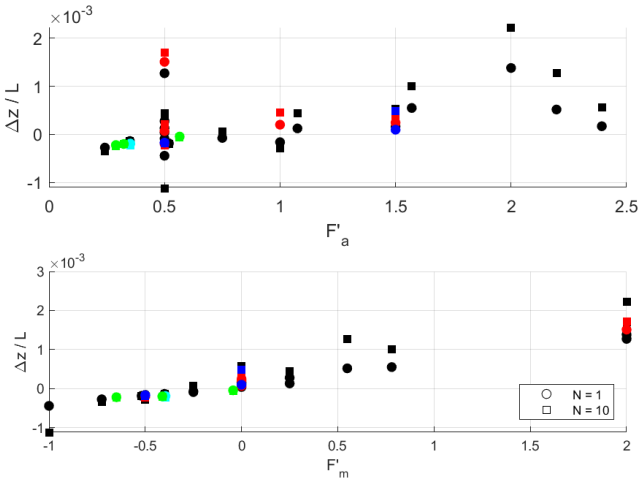

Figure 5. Normalized displacements after N = [1,10] cycles by load configuration.

Figure 6 shows the displacements for $\Delta z^* = \Delta z - \Delta z_{N=1}$ normalized by the caisson skirt length. As also shown in (Sanders and Achmus, 2023), only tests in which the load exceeded the drained tensile capacity showed significant displacements.

Amplitude and frequency had a major influence for the behavior at higher number of cycles. For tests with $F'_m = -0.5$ and $F'_a = 0.5$ (♦) the lower frequency had a destabilizing effect. Yet, also the higher frequency test showed slightly higher displacements than the base case. In tests with $F'_m = 0$ and $F'_a = 1.5$ (x), again the lower frequency had a negative effect. All three tests with this load combination experienced settlements initially. For the test with $f = 1\,Hz$ the heave displacements occurred after a much higher number of cycles and the test with $f = 3\,Hz$ experienced exclusively settlements.

Interestingly, an inverse pattern can be seen for tests with $F'_m = 0$ and $F'_a = [0.5, 1.1, 1.5, 2.3]$, in which higher amplitudes lead to greater rates of settlement initially and heave displacements at lower number of cycles, even though higher load amplitude implicates higher load application rates. Additionally, in these tests smaller amplitudes lead to smaller settlements during cycles until heaves occurred.

Thus, not only the load application rate but also the absolute load magnitude had a significant influence.

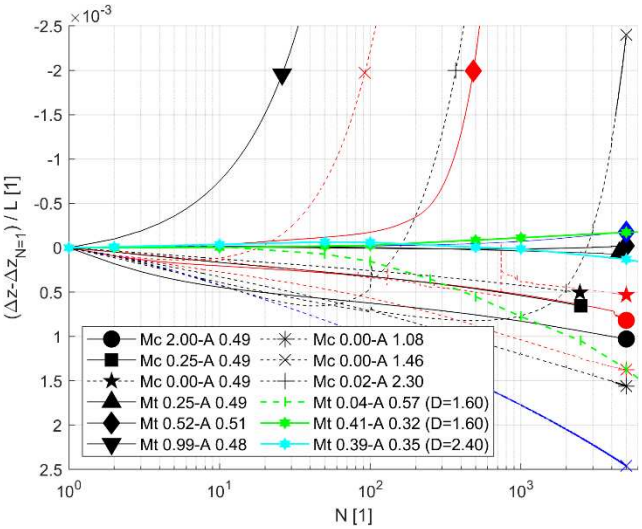

Figure 6. Normalized displacements observed in small and large scale model tests. Mt and Mc denote tensile and compressive mean load, respectively.

3.3 Influence of the scale

Three sets of small-scale model tests with loading conditions similar to those of the large scale model tests were performed to compare the displacement-behavior of tests at different scales. First, a test with approximately $F'_m = -0.4$, $F'_a = 0.35$ and $f = 1$ Hz was performed at the small scale. Then, tests with $F'_m = 0$, $F'_a = 0.5$ and $f = [1\ 0.33]$ Hz are compared to a large scale test with $F'_m = -0.04$, $F'_a = 0.57$. Since $F'_{min} < -1$ for all these tests, they were expected to show no significant heave displacements. The results are presented in detail in figure 7.

Interestingly, the large scale tests with $F'_m = -0.4$ and $F'_a = 0.35$ (i.e. $F'_{min} = -0.75$) showed smaller displacements than the test with $F'_m = 0.04$ and $F'_a = 0.57$ ($F'_{min} = -0.61$). This might be explained by the fact that for the latter test, loading was the first load package while for the other two the shown load packages were the 2nd and 4th, respectively. The nature of the pure settlements does though fall in line with the small-scale test results.

All three tests with mean tensile load experienced initial heave displacements. The large scale model with D_1 experienced further heave displacements afterward while the test with D_2 after approximately $N = 100$ cycles only experienced settlements. The small-scale test experienced exclusively settlements after the initial upward displacement.

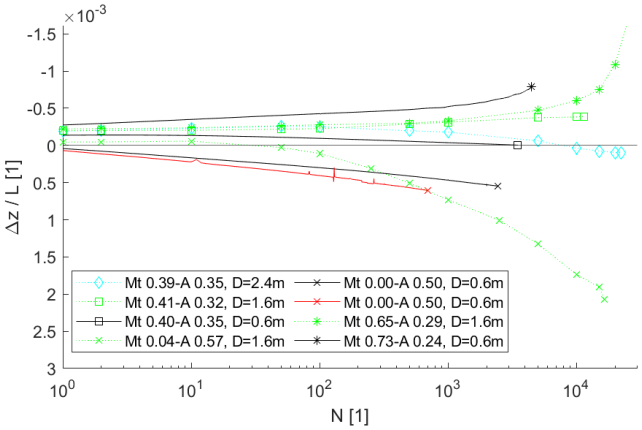

Figure 7. Displacements observed in small and large scale model tests for two sets of tests with similar loading conditions.

All tests with $F'_m = 0$ experienced settlements after larger number of cycles with the large scale model test showing the greatest displacements. All small-scale model tests (c.f. figure 6) with $F'_m = 0$ show initial settlements, which could have been caused by the initial loading in compression. The settlement over larger number of cycles for small-scale model tests and the settlements observed in the large scale model test after initial heaves due to initial tensile loading indicate that indeed the settlements are caused by the load configuration and not the initial loading direction. In all small- and large scale model tests, cyclic loading with $F'_m \leq 0$ did not lead to heave displacements. Yet, this behaviour can be caused by initial compaction of the soil and might be limited to certain numbers of cycles. Furthermore, this favorable behavior might be impeded by load configurations with high load amplitudes even when $F'_m = 0$.

Initial settlements were no guarantee for limited heave displacements at higher number of cycles.

3.4 Pore water pressures in small-scale model tests

Figure 8 shows the pore water pressures measured during cycling at the lid invert. Mean pore water pressures occur during the first loading cycles, with a high dependency on mean load and a subordinate dependency on the loading amplitude, indicating the dependency on the drainage conditions of the system. Only one test with $F'_m = -1.0$ and $F'_a = 0.5$ (i.e. $F'_{min} = -1.5$, ▾) showed accumulated pore water pressures from the first cycle on.

Mean pore water pressure decayed in all test after $N = 2$ cycles. In some cases, pore water pressures beneath the lid changed sign from their initial state. This was present for most, but not exclusively in, tests with $F'_m = 0$.

After approximately $N = 50$ to $N = 100$ cycles, the minimum mean pore water pressures were achieved. For some tests, the magnitude of mean pore water pressure again increased slightly, especially in tests that showed greater displacements. Again, this was no clear indicator for ongoing displacements.

The observed accumulations were rather an expression of heave displacements than an indication towards upcoming heaves. The trend for heave displacements was visible at much lower number of cycles than the accumulations of mean pore water pressure.

Even though loading frequency and amplitude load have a decisive influence on the displacement behavior, no clear indication of this influence could be made out in accumulated pore water pressures.

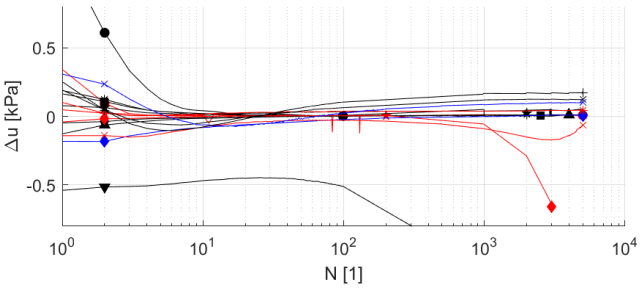

Figure 8. Mean pore water pressures at lid invert during cyclic loading of all small-scale model tests. Negative values indicate suction.

3.5 Post-cyclic drained tensile capacity

Figure 9 shows the resistance factor deduced from pre- and post-cyclic drained tensile capacity ($k{\cdot}tan(\delta)_{t,pre}$ and $k{\cdot}tan(\delta)_{t,post}$) for all small model scale tests.

All but one test in which $F_{dr,t}$ could be determined showed an increase in drained tensile capacity. The test with $F'_m = 0$, $F'_a = 1.5$ and $f = 0.33$ Hz showed a significant decrease in $F_{dr,t,post}$ of about 63% due to high heave displacements. Yet the resistance factor increased due to the lower embedment length. For some tests with very high heave displacements no value was obtained ($N_{max} < 5000$).

A correlation between change in resistance factor and both loading amplitude and mean load can be seen. With increased loading amplitude, the resistance factor increased, too. While stronger tensile mean load lead to lower increase in resistance factor, compressive mean loads had a similar effect regardless of their magnitude.

The increase in capacity might explain, why some tests with maximum tensile loads in the magnitude of the drained tensile capacity do not show ongoing heave displacements for a large number of cycles. Also, compaction of the soil for tests with zero mean load can cause settlements after initial loading.

While an increase in the drained tensile capacity was observed, it is not clear whether this observation is valid for very large number of cycles or all load combinations.

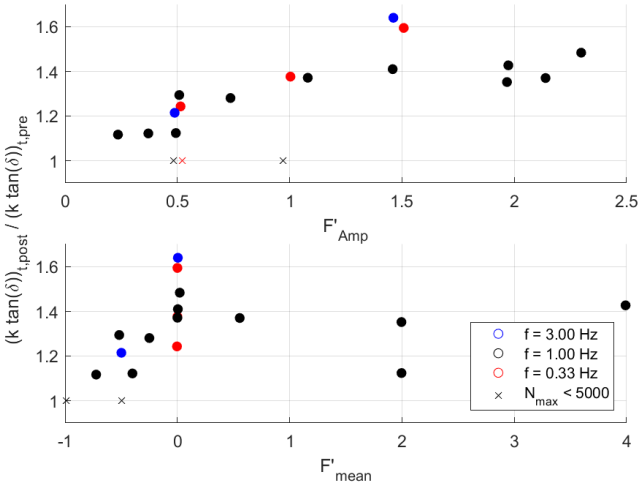

Figure 9. Change in resistance factor from drained tensile capacity after cyclic loading. x – no determination of post-cyclic resistance factor due to excessive heave displacements.

4 CONCLUSIONS

In this study, 1g model tests on suction caissons with diameters $D = [0.61, 1.60, \text{and } 2.40]$ m were compared. No indication could be found that pore water pressure accumulation is a driver for vertical displacements of the caissons, it rather indicated displacements that had already occurred. For loads that did not exceed the drained tensile capacity, displacements were rather small. An increase in drained tensile capacity after the applied 5000 cycles was found in most of the small-scale model test but was dependent on the loading conditions.

While the mean load mainly influenced displacements and pore water pressures during the first cycles, the loading amplitude was the main influencing factor for behavior at larger numbers of cycles and an increase in drained tensile resistance factor.

After initial heave displacements, settlements were observed on all geometric scales even for tests with a tensile mean load. This was attributed to soil recompaction as also indicated by the increased drained tensile bearing factor observed in small scale tests. It was concluded, that trends in displacement observed in 1g small-scale model tests were applicable to several geometric scales.

The results indicate that small tensile mean loads might be admissible for suction caissons, as long as loading amplitude and number of cycles with such loading conditions are limited.

AUTHOR CONTRIBUTION STATEMENT

Immo Sanders: Conceptualization, Methodology, Investigation, Data curation, Visualization, Writing – original draft, review & editing. **Martin Achmus**.: Conceptualization, Funding acquisition, Supervision, Writing – review & editing. **Dariya Heinrich**: Investigation, Data curation, Writing – review & editing. **Tulio Quiroz**: Investigation, Project administration, Writing – review & editing. **Waldemar Elsesser**: Writing – review & editing

ACKNOWLEDGEMENTS

The work presented in this contribution was carried out within the ProBucket project. The authors kindly acknowledge the financial support provided by the German Federal Ministry of Economic Affairs and Climate Action (FKZ 03EE3033). The support provided by the project partners is also gratefully acknowledged.

REFERENCES

Bienen B., Klinkvort R.T., O'Loughlin C.D., Zhu F., and Byrne B.W. (2018). Suction caissons in dense sand, part II: vertical cyclic loading into tension. Géotechnique 68(11):953–967. https://doi.org/10.1680/jgeot.16.P.282

Byrne B.W. (2000). Investigations of suctino caissons in dense sand. Ph.D. Thesis, University of Oxford, Oxford, United Kingdom.

Gütz P. (2020). Tensile-loaded suction bucket foundations for offshore structures in sand. Ph.D. Thesis, Leibniz University Hannover, Hannover, Germany. https://doi.org/10.15488/10152

Heinrich D., Quiroz T., Elsesser W., Schädlich B., and Sanders I. (2025). Evaluating calculation methods for suction-assisted installation techniques in dense sand: a comparative study. In: 5th International Symposium on frontiers in offshore geotechnics Proceedings, Nantes, France.

Hettler A. (1982). Approximation formulae for piles under tension. In P. A. Vermeer and H. J. Luger, editors, Deformation and failure of granular materials, pages 603–608. Balkema, 1982, ISBN 90-6191-224-5

Kelly R.B., Byrne B.W., and Martin C.M. (2004). Tensile Loading of Model Caisson Foundations for Structures on Sand. In: The proceedings of the Fourteenth (2004) International Offshore and Polar Engineering Conference, ISOPE-2004. Cupertino, USA, pp. 638 – 641.

Kelly R.B., Houlsby G.T., and Byrne B.W. (2006). Transient vertical loading of model suction caissons in a pressure chamber. Géotechnique56(10):665-675. https://doi.org/10.1680/geot.2006.56.10.665

Lombardi D., Cox J.A., and Bhattacharya S. (2011). Long-term performance of offshore wind turbines supported on monopiles and suction caissons. In: 8th Int. Conf. on Structural Dynamics Proceedings, Leuven, Belgium.

Sanders I. and Achmus M. (2023). On the behaviour of suction caissons under cyclic axial loading, In: Offshore Site Investigation Geotechnics 9th International Conference Proceeding, London, United Kingdom, pp. 1781-1788. https://doi.org/10.3723/DKKK3850

Stapelfeldt M., Bienen B., and Grabe J. (2020). The influence of the drainage regime on the installation and the response to vertical cyclic loading of suction caissons in dense sand. Ocean Engineering 215:107105. https://doi.org/10.1016/j.oceaneng.2020.107105

Vaitkunaite E. (2016). Physical Modelling of Bucket Foundations Subjected to Axial Loading. Ph.D. Thesis, Aalborg University, Aalborg, Denmark. https://doi.org/10.5278/VBN.PHD.ENGSCI.00119

Wood D.M. (2004). Geotechnical Modelling, 1st ed., Taylor & Francis Ltd, London, United Kingdom. https://doi.org/10.1201/9781315273556

Zhang Y., Sudhakaran K., Askarinejad A. (2020). Centrifuge Modelling of Suction Caissons Subjected to Cyclic Loading in Tension. In: The Proceedings of the 4th European Conference on Physical Modelling in Geotechnics, ECPMG 2020. Luleå, Sweden, pp. 263 – 268.